NANO MICRO small

Peptidic Ligands to Control the Three-Dimensional Self-Assembly of Quantum Rods in Aqueous Media

*Thomas Bizien, Pascale Even-Hernandez, Marie Postic, Elsa Mazari, Soizic Chevance, Arnaud Bondon, Cyrille Hamon, David Troadec, Ludovic Largeau, Christophe Dupuis, Charlie Gosse, Franck Artzner, and Valérie Marchi**

***T**he use of peptidic ligands is validated as a generic chemical platform allowing one to finely control the organization in solid phase of semiconductor nanorods originally dispersed in an aqueous media. An original method to generate, on a macroscopic scale and with the desired geometry, three-dimensional supracrystals composed of quantum rods is introduced. In a first step, nanorods are transferred in an aqueous phase thanks to the substitution of the original capping layer by peptidic ligands. Infrared and nuclear magnetic resonance spectroscopy data prove that the exchange is complete; fluorescence spectroscopy demonstrates that the emitter optical properties are not significantly altered; electrophoresis and dynamic light scattering experiments assess the good colloidal stability of the resulting aqueous suspension. In a second step, water evaporation in a microstructured environment yields superstructures with a chosen geometry and in which nanorods obey a smectic B arrangement, as shown by electron microscopy. Incidentally, bulk drying in a capillary tube generates a similar local order, as evidenced by small angle X-ray scattering.*

Dr. T. Bizien, Dr. P. Even-Hernandez, Dr. S. Chevance, Dr. A. Bondon, Dr. C. Hamon, Dr. V. Marchi
Université de Rennes 1, CNRS UMR 6226
Institut des Sciences Chimiques de Rennes
Avenue du Général Leclerc 35042, Rennes, France
E-mail: valerie.marchi@univ-rennes1.fr

Dr. T. Bizien, Dr. M. Postic, Dr. F. Artzner
Université de Rennes 1, CNRS UMR 6251
Institut de Physique de Rennes
Avenue du Général Leclerc
35042, Rennes, France

Dr. E. Mazari, Dr. L. Largeau, C. Dupuis, Dr. C. Gosse
Laboratoire de Photonique et de Nanostructures
LPN-CNRS, Route de Nozay 91460, Marcoussis, France

Dr. D. Troadec
Institut d'Electronique
de Microélectronique et de Nanotechnologie (IEMN)
CNRS UMR 8520, Cité Scientifique
59655, Villeneuve d'Ascq, France

DOI: 10.1002/smll.201400300

1. Introduction

Anisotropic semi-conductor nanocrystals, as well as their collective assemblies, have emerged as a promising class of materials owing to their unique size- and shape-dependent optical properties.[1] In particular, core/shell quantum rods (QRs) challenge their quantum dots (QDs) counterparts for energy conversion[2] and light harvesting, due for example to their longer exciton lifetime and to the linear polarization that appears along their main axis under irradiation.[3]

Nevertheless, succeeding in the fabrication of functional devices still depends on our ability to integrate QRs on a macroscopic level. More specifically, the use of these nano-objects as building blocks to develop complex ordered structures—via a 'bottom-up' approach—necessitates to precisely tune interactions between particles and thus to perfectly control the surface chemistry of the individual crystallites. In addition, it would be valuable for any proposed technology to be low-cost and green. Only a few reported methods yielded

three-dimensional (3D) features.[4] The simplest method consisted in allowing an organic QRs suspension to evaporate until a supracrystal is formed, the atmosphere being saturated with solvent.[1b,5] Although representing a significant advance, this process may in the future lack of flexibility because colloidal behavior in organic phase is not as rich as in water. Previously, we have described an original strategy for shaping self-assemblies of gold nanorods (GNRs) by slow drying of the corresponding aqueous solution between a smooth substrate and a topologically micropatterned mold. Walls displaying a smectic B packing were then obtained, organized on a regular lattice over several square millimeters.[6] Moreover, the spacing between particles could be varied by adjusting their surface charge and thus their interaction potential. Finally, our technique did not require expensive equipment and was environmentally friendly because it mainly involved water evaporation. As a consequence, these promising results prompted some implementation with core/shell semi-conductor nanorods.

At the end of the synthesis, QRs are coated with hydrophobic ligands; hence, post-synthetic surface engineering is compulsory to obtain hydrophilic objects. Importantly, during this procedure one has to preserve both the colloidal stability and the photoluminescence properties of the nanocrystals. The different strategies, that have been described for preparing water-soluble nanorods from hydrophobic ones, include coating chemical modification,[7] polymer layer addition,[8] silanization,[9] cap exchange[10] and micellar encapsulation.[7b] In the latter approach, peptides appear as very attractive ligands since their chemical structure can easily be devised to strongly bind the QR surface and to generate electrostatic and hydrophobic interparticle forces that are well balanced.[11] It is also worth noting that those derivatives can advantageously be purchased from commercial providers, thereby avoiding one to engage itself in time-consuming synthesis. To the best of our knowledge, only one single example of peptides grafting onto semi-conductor rod-shape particles has been published.[12] As a matter of fact we then largely built on our own experience with QDs.[11,13] For instance, although several bidentate molecules, such as lipoic acid[14] and histidine amino acids,[15] have been proved to exhibit a fair affinity to semiconductor surface, we here favored species bearing a tri-cysteine moiety because we had previously shown that they yield a strong binding, resulting in stable aqueous suspensions.[13] Concerning the various functional groups and spacers that can be introduced in the amino acid sequence, one can for instance rely on an alkyl chain to increase the ligand packing density. Conversely, an ethylene glycol spacer will promote solubility in water and generate a steric repulsion able to prevent aggregation. Moreover, ionizable groups grafted in terminal position, such as carboxylic acids or amines, will allow one to tune the particle charge. All in all, it will therefore be possible to design ligands that are optimized to stabilize nanorods in aqueous solution and that yield a final material with precisely defined properties.

To achieve the present study, we relied on CdSe/CdS nanorods because they can be synthesized with a high monodispersity and with variable aspect ratio.[16] Furthermore, for the sake of clarity our approach is here demonstrated by focusing on a single peptide, although various molecular structures have revealed themselves functional during our research. The crucial role of the coating for successful 3D self-assembly has motivated the utilization of a large set of techniques to understand binding events at the nanoparticle surface during the ligand exchange process.[6] More precisely, fluorescence,[17] infrared (FTIR),[18] and nuclear magnetic resonance (NMR) spectroscopies[19] enabled us to show that the hydrophobic phosphorylated molecules serving for the QR capping, the octadecyl phosphonic acid (ODPA), the hexyl phosphonic acid (HPA), as well as the tri-octyl phosphine oxide (TOPO) and the tri-octyl phosphine (TOP), can be completely replaced by peptides. Subsequently, we accessed the surface charge of the hydrophilized QRs, as well as their stability in water, by electrophoresis and by dynamic light scattering (DLS). Ligand exchange methods usually suffer from a strong decrease of quantum efficiency. Accordingly we also checked that the fluorescence intensity of the hydrophilized QRs is vanished only by a factor of 2, which provides a brightness still in comparison to the one of much of the organic fluorophores solubilized into water.[20] Finally, structural data on 3D assemblies were obtained thanks to two complementary experimental approaches: bulk colloidal crystal dried in capillaries tubes were analyzed by small angle X-ray scattering technique (SAXS) whereas wall features resulting from casting and evaporating a QR suspension between a substrate and a polydimethoxysilane (PDMS) stamp were investigated by both scanning and transmission electron microscopies (SEM and TEM, respectively).

2. Results

The highly monodisperse CdSe/CdS nanorods used in this work were grown following the seeded approach described by Carbone et al.[21] After purification from ligands in excess, hydrophobic QRs were obtained dispersed in toluene. The length and diameter of these particles were determined by TEM to be 17.9 ± 0.7 and 6.7 ± 1.2 nm, respectively (see Figure S1a, Supporting Information). Furthermore, the wurtzite structure was confirmed by analysis of the STEM-HAADF images, the nature of the seed as well as the one of its surrounding were identified thanks to the characteristic and slightly different crystallographic parameters of CdSe and CdS (see Supporting Information Figure S1b and Table S1).[21] Finally, the UV–vis absorption spectrum in toluene exhibits three characteristic peaks corresponding to the absorption of the core at 580 nm and of the anisotropic shell at 421 and 471 nm. Conversely, the fluorescence emission spectrum obtained upon excitation at 390 nm displays a single sharp peak centered at 585 nm (see Figure S1c, Supporting Information), which is associated to the sole seed and which quantum yield Φ_{QR} was estimated to be ~ 0.45.

2.1. Ligand Exchange Characterization

As described in **Figure 1**a, hydrophobic QRs were made hydrophilic by replacing the phosphorylated ligands issued

small 2014,
DOI: 10.1002/smll.201400300

NANO MICRO small

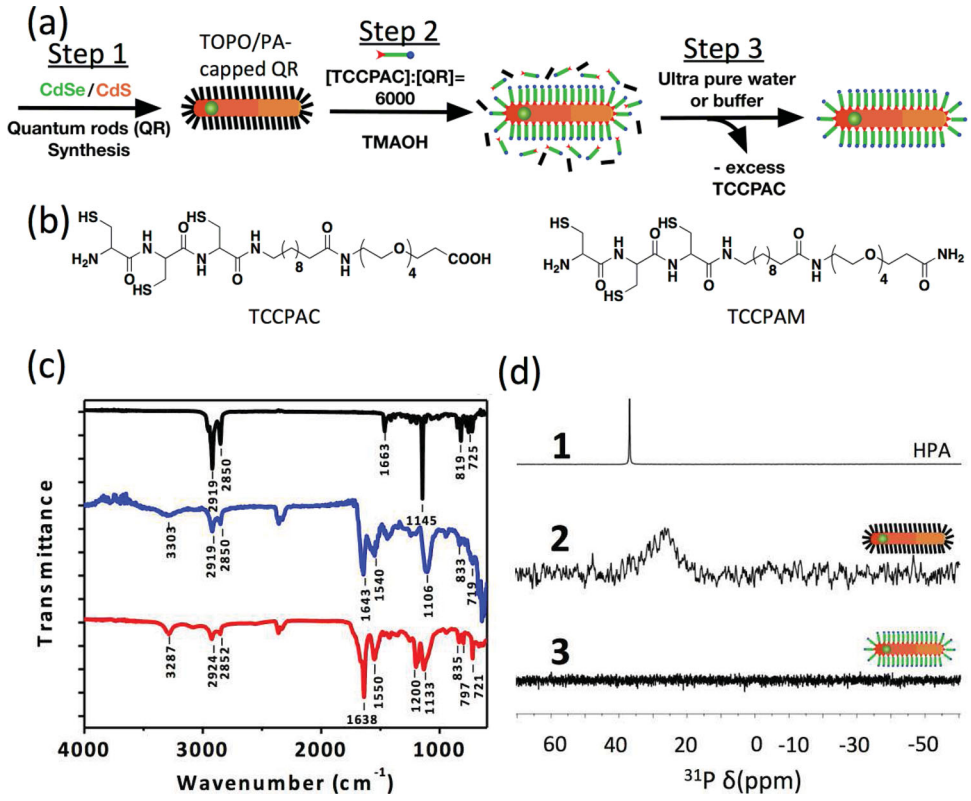

Figure 1. a) Schematic view of the whole process yielding peptide-QRs, from nanoparticles synthesis in organic solvent to ligand exchange and purification of the hydrophilic colloids. b) Chemical structure of the TCCPAC and TCCPAM peptides. c) FTIR spectra of the hydrophobic QRs (black), of the TCCPAC ligand (red), and of the TCCPAC-QRs (blue). d) ^{31}P NMR spectra in $CDCl_3$ of the hexyl-phosphonic acid (1), of hydrophobic QRs (2) and of peptide-QRs (3). For the latter measurements excess ligands was removed by centrifugation/redispersion in toluene/methanol or by size exclusion chromatography.

from the synthesis by the TCCPAC peptide. The molecular structure of the latter compound is given in Figure 1b. An alkyl chain length of eleven carbon atoms was introduced to get a high lateral attractive Van der Waals interaction within the coating layer. On the other hand, a PEG spacer was inserted. It was selected long enough to get a good solubility of the particles in water and to generate Helfrich undulation repulsive forces that ensure a satisfactory colloidal stability.[1,22]

In practice, purified hydrophobic nanorods dissolved in chloroform were incubated in presence of a large excess of peptide solubilized in pure water. TMAOH was also added as a phase transfer agent. After 20 minutes of incubation, QRs have left the organic phase for the aqueous one. These water-soluble peptide-capped QRs, now denoted TCCPAC-QRs or more generally peptide-QRs, were then purified by size exclusion chromatography to eliminate the peptide in excess as well as traces of any other reagents.

To investigate the nature of the ligands at the nanorods surface, FTIR analyses were carried out first (Figure 1c). When comparing the data associated with hydrophobic QRs to the ones issued from peptide-QRs we note that the peaks corresponding to the phosphoryl P=O band at 1145 cm^{-1} and to the hydrogen phosphoryl P–OH band at 819 cm^{-1} have disappeared during the cap exchange. They were indeed related to the ODPA and to the HPA, as well as to the TOPO and to the TOP. By contrast, the emergence of the amide carbonyl C=O band at 1643 cm^{-1} clearly indicates the presence of TCCPAC. The four hydrophobic ligands have been replaced by the peptide.

To further prove the quantitative nature of ligand substitution at the QR surface, we relied on both ^{31}P and ^{1}H NMR spectroscopies.[23] More precisely, we selected the former technique because it is generally used to characterize the capping of CdSe/CdS nanoparticles synthesized in mixtures of phosphonic acids such as HPA and ODPA.[24] These molecules are usually strongly coordinated to the semiconductor surface and their signal therefore appears as a very broad peak. Indeed, the decrease of the molecular motions close to the solid interface yields more efficient relaxation pathways.[25] Similar observations were obtained here: whereas the pure HPA spectrum exhibits a very sharp feature, the hydrophobic QR spectrum shows a very broad resonance centered at 27 ppm (see Figure 1d). After ligand exchange, phase transfer, and purification by size exclusion chromatography, we obtain an aqueous suspension of peptide-QRs that does not exhibit a phosphorus signal anymore. As far as ^{1}H NMR is concerned, full signal assignment for the TCCPAC peptide was first performed using standard procedures, both for the 1D (see Figure S2a,b, Supporting Information) and for the 2D spectra (see Figure S3, Supporting Information). It is worth noting that the chemical shifts of the peaks corresponding to the three Hα of the cysteines are sensitive to the pH due to the acido-basic properties of the thiols (see

DOI: 10.1002/smll.201400300

Figures S2b and S2c). On the other hand, the ^{1}H spectrum of TCCPAC-QR exhibits two peaks at 3.7 ppm (H14) and 4.3 ppm (H15/H16) that can be attributed to the cysteine protons of the free peptide in solution at pH 9.0 before size exclusion chromatography (see Figure S4, Supporting Information). This latter observation indicates the presence of an excess of free TCCPAC. After purification, these peaks vanish in agreement with the elimination of the free peptide (see Figure S4, Supporting Information). In addition the peaks attributed to TMAOH (at 2.8 ppm and 3.0 ppm), methanol (around 3.2–3.3 ppm) and phosphorylated ligands also disappear (see Figure S4, Supporting Information). These results are in good agreement with the previous FTIR data and comfort the observation of a quantitative cap replacement. The observations made on ^{1}H NMR spectra also demonstrate that the purification by size exclusion chromatography is efficient to remove the large excess of peptide required for ligand exchange.

Additional data could be obtained using diffusion ordered spectroscopy (DOSY),[25] a technique which discriminates the resonances of the free and bound peptides according to their molecular diffusion.[26] When analyzing purified TCCPAC-QRs we found that the protons of the PEG portion as well as the ones of the first methylene group (H9) are associated with a 0.44 10^{-10} m^2 s^{-1} diffusion coefficient. This value is significantly lower than the 1.35 10^{-10} m^2 s^{-1} one obtained for all the peaks of free TCCPAC in the region from 1 to 4 ppm (see Figure S5, Supporting Information). These latter results confirm the attachment of the peptide to the nanorod surface.

We could further quantify the binding of the peptidic ligand to the CdS surface by monitoring the modifications of its 1D ^{1}H NMR spectrum during the addition of a solution of purified TCCPAC-QRs to a solution of TCCPAC (see **Figure 2**a and SI for further details). The sharp peaks of the free peptide initially present vanish during titration since more and more unsaturated QR surface is available for binding. The integrated area of the cysteine Hα peaks (H15/H16) decreases until completely disappearance. Conversely, during the addition of a solution of free TCCPAC peptide to a purified peptide-QR suspension, all the characteristic peaks of the free peptide are recovered at a titrant concentration of 4.4 mM, corresponding to the point where the saturation of the QR surface is achieved (see Figure 2a). In both cases, the most affected signals (shadowed on the spectra of Figure 2a) concern the three-cysteines residues (H6–9 and H15/16). The signals of the H2 and H9 protons located at the beginning of the flexible side chain of the ligand are broadened to a lesser extend in agreement with a greater mobility of the alkyl chain. Thus, the evolution of these peaks strongly suggests an anchoring through the cysteine residues. In addition this experiment also provides an estimation of the number of peptides per QR. Indeed, during the addition of peptide-QRs to a solution of free TCCPAC, the integration area of the peaks H1 and H4, belonging to the ligand alkyl chain, as well as H12 belonging to the PEG moiety, are fully correlated with the increasing amount of nanoparticles (see Figure 2b). More precisely, with the help of an external standard, the integrations are directly converted into concentrations. More precisely integrated values vary respectively from 64 to 83 (H1), from 16 to 19 (H4), and from 74 to 83 (H12), increasing from about 20%. Knowing the starting amount of free peptide, it is thus possible to extract the amount of peptides present on the TCCPAC-QRs. From the QR concentration, the estimation of the ratio of peptides per QR is roughly evaluated to be around 650 after ligand exchange. The QR surface area (360 nm^2) is estimated by considering the QR (of length 18 nm and diameter 5 nm) as a cylinder closed with two half spheres at its extremities. We can deduce the mean surface occupied by one peptide to be around 0.6 nm^2. As anticipated, this result shows that the surface of hydrophilic QRs is not totally saturated with peptides after ligand exchange.

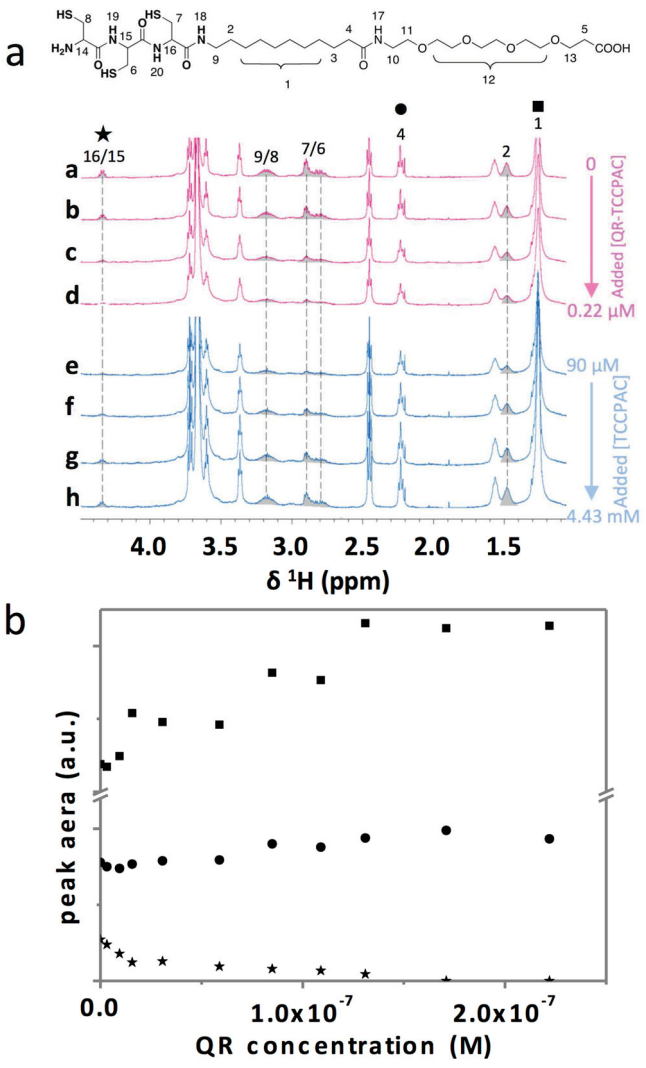

Figure 2. a) ^{1}H NMR spectra during the addition of the purified TCCPAC-QRs to a solution of free TCCPAC peptide and reverse. First, peptide-QRs were progressively added up to 0.22 µM (pink spectra) and then the mixture was supplemented little by little with free TCCPAC peptides, up to 4.43 mM (blue spectra). The most affected signals are shadowed and their intensity evolution during the titration experiment is followed by dotted lines: they belong to the three-cysteine residues (peaks 16/15, 9/8, 7/6) or to the proton 2 located very close to these anchoring residues. b) Evolution of signal intensity during the first titration: (*) Hα protons 16/15 belonging to the cysteine residues, (●) H4 and (■) H1 belonging to of the alkyl chain.

small 2014,
DOI: 10.1002/smll.201400300

NANO MICRO small

2.2. Properties of Peptides-QRs in Aqueous Solution

Nanorods self-assembly and the use of the obtained materials for applications in optics[27] or in energy conversion[2] impose to use particles initially well dispersed in solution, which display a controlled surface chemistry and a preserved fluorescence emission. An overview of the purified TCCPAC-QR optical and colloidal properties is given in **Figure 3**. We measured absorbance and fluorescence emission spectra similar to the hydrophobic QR ones (compare Figure 3a and Supporting Information Figure S1c). However, the fluorescence quantum yield Φ_{QR} has been proved to decrease from 0.45 to 0.20 upon ligand exchange. This change might be attributed to the trapping of the photo-induced charge separation by interactions with the polythiolate ligands at the inorganic crystal surface. Additionally, TCCPAC-QRs are photostable for weeks as soon as pH is higher than 4 (see Figure 3b). At pH 3, fluorescence intensity falls to nearly zero after 3 days, a phenomenon that we attribute to aggregation. Indeed, it correlates with a dramatic increase of the average hydrodynamic diameter measured by DLS (see Figure 3c).

To gain more insight on the influence of the ligand structure on particle properties, we relied on two additional peptides. First we modified the QR surface charge by mixing TCCPAC with TCCPAM, the parent molecule bearing a terminal amide group instead of a carboxylic acid one (see Figure S6a). For all the investigated capping mixtures nanorods migrate as a single and well-defined band in agarose gel electrophoresis, which indicates that colloidal stability was always preserved (see Figure S6b). As expected, we also noticed an electrophoretic mobility increasing with the TCCPAC/TCCPAM ratio. Similar results have previously been observed for QDs coated with PEGylated peptidic ligands[11] and for GNRs coated with PEGylated alkyl thiolate ligands.[6] In a second set of experiments, we introduced TCPAC, a peptide similar to TCCPAC although it does not include the alkyl chain (see Figure S7a). Fluorescence and DLS data revealed that both photophysical and colloidal stabilities were much smaller under acidic conditions. On the long term, aggregation was even observed for neutral and basic pH (see Figure S7a and b). The colloidal stability of the nanoparticles decreases if the free peptide concentration in the QR suspension decreases (data not shown). As the peptide ligand possesses a strong affinity to the QR surface, this effect is limited by the slow kinetics of the peptide desorption. Thus, the presence of an alkyl chain seems to be a key factor in the design of ligands able to provide a good QR dispersion in aqueous solutions.

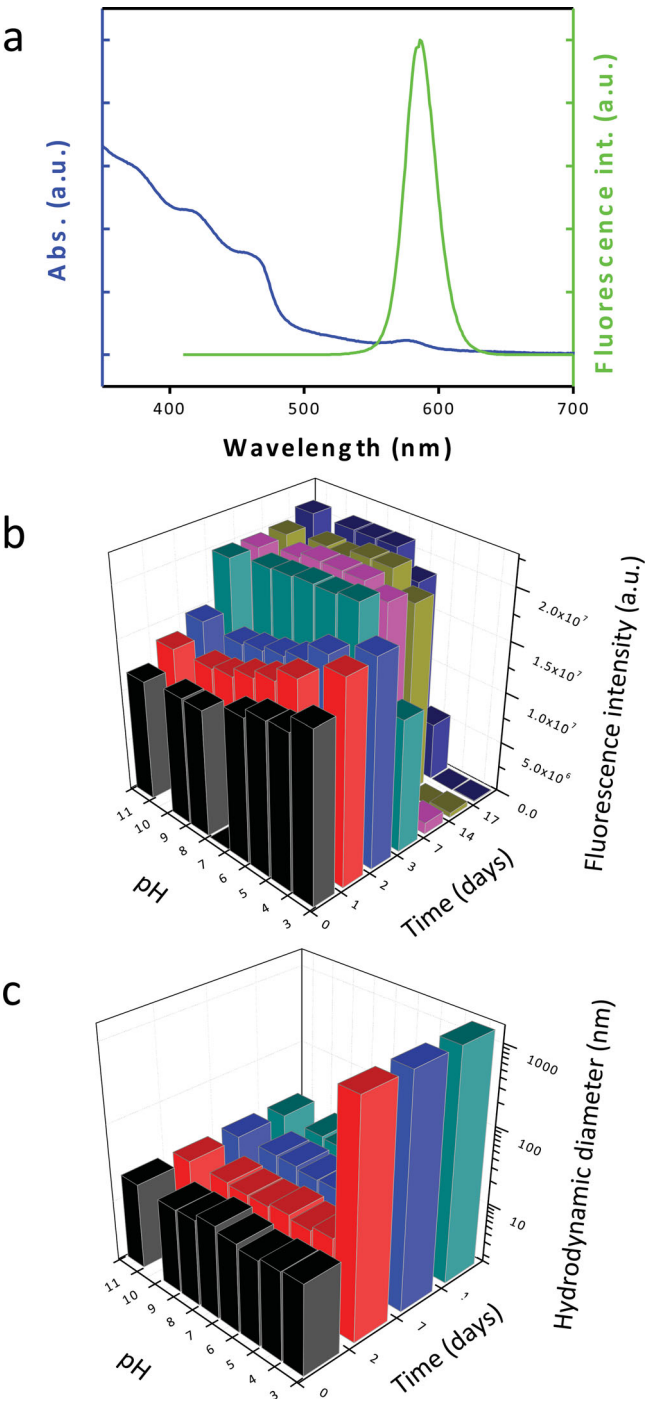

Figure 3. Characterization of the purified TCCPAC-QRs. a) Normalized absorbance and fluorescence spectra in ultra pure water. b) Evolution in time of the fluorescence intensity for TCCPAC-QRs dissolved at 1 nM in Britton and Robinson buffers with a 20 mM ionic strength and which pH adjusted to various values between 3 and 11. c) Evolution in time of the hydrodynamic diameter for the previous TCCPAC-QR solutions, measurements were performed by DLS after a hundredfold dilution.

2.3. Peptide-QR Self-Assembly

In view to integrate nanorods into devices, we explored a controlled drying method yielding well-defined patterns of auto-organized superstructures.[6] More precisely, an aqueous suspension of TCCPAC-QRs was first confined between a flat substrate and a PDMS stamp before water was allowed to evaporate freely (see **Figure 4**a,b). After removal of the elastomeric mold, a macroscopic array of linear and circular features was obtained, as demonstrated by optical fluorescence and scanning electron microscopies (see Figure 4c–e, respectively). SEM images clearly reveal that QRs are densely packed within these walls. For instance, some hexagonal arrangement is observed normal to the superstructure surface (see Figure 4f). Additionally, a lamellar organization

DOI: 10.1002/smll.201400300

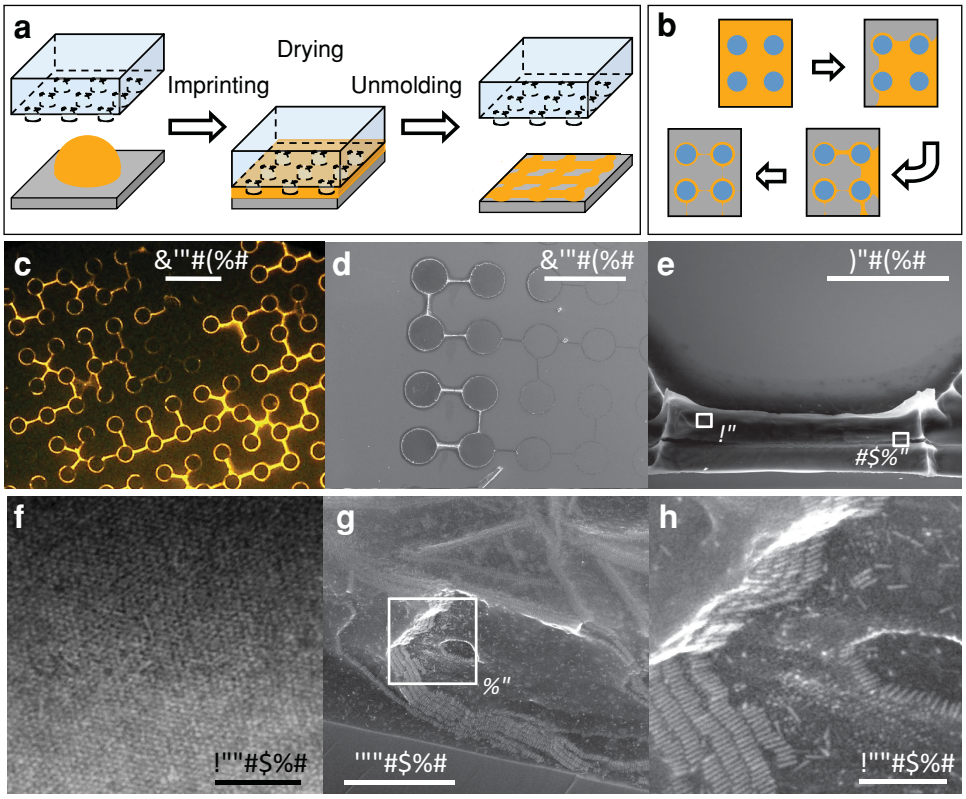

Figure 4. a) Schematic view of the method used to fabricate superstructures made of self-assembled TCCPAC-QRs. b) Schematic explanation for the formation of walls upon solvent evaporation and contact line pining. c) Typical epifluorescence image of the obtained features square array. d,e) Corresponding SEM views. Letters indicate the location of the following magnifications: f) Hexagonal QR packing observed normally to the wall surface. g,h) Smectic B organization revealed upon resection of a piece of supracrystal.

is evidenced in places where a part of colloidal crystal has been fortuitously removed during cleaving (Figure 4g,h). Thereby, we can infer the existence of a local smectic B order. To get quantitative measurements of the lattice parameters, thin foils were micromachined by focussed ion beam (FIB) perpendicularly to the wall ridge and inspected by STEM-HAADF (see **Figure 5**a). Fourier analysis of QRs assemblies seen along the particles main axis gives a hexagonal parameter $a_{SmB} \approx 87 \pm 6$ Å (Figure 5b,c). The measurement of the intensity profile acquired along a raw of QRs seen in a lamellae cross-section gives a less accurate estimation of the lateral interdistance (80 ± 10 Å) but validates the previous result (see Figure 5d,e).

To further explore the ability of TCCPAC-QRs to self-organize upon water evaporation, SAXS was used to analyze the solid obtained from drying a colloidal suspension in a glass capillary. Peak indexation indeed confirmed the existence of a smectic B crystal phase, as shown in **Figure 6** (see also Table S2, Supporting Information). The unit cell parameters are a = 97.6 Å and c = 638 Å, they correspond to a hexagonal spacing $a_{SmB} = a$ = 97.6 Å and to a lamellar repeat distance $d_{SmB} = c/3$ = 212.6 Å. Those data are thus in fair agreement with the ones obtained by STEM-HAADF.

Incidentally, we noticed that organic solvent evaporation from a suspension of hydrophobic QRs also yields a smectic B crystal phase. Its lateral interdistance and lamellar repeat distance are $a = a_{SmB}$ = 68.6 Å and $c = d_{SmB}$ = 168.9 Å, respectively (see Figure S9, Supporting Information). Hence, grafting of TCCPAC peptides induces an increase of about 30 to 50 Å for these parameters. The SAXS spectrum from the sample originally in organic solvent exhibited also a lower interlamellar and lateral order than the one from the sample dried from water. It may be due to the negative charges at the nanorod surface, which can favor interparticle repulsion, and/or to the alkyl chain in the ligand structure, which can harden the interaction potential because of crystallization inside the coating.

3. Discussion

The present experiments clearly demonstrate the ability of core/shell quantum rods to self-assemble into a smectic B phase upon colloidal suspension drying. This operation was achieved in water after initial phosphorylated ligands had been exchanged for peptides with precisely devised properties. More specifically, we first showed by FTIR and NMR spectroscopies that a simple 'mix-and-react' protocol can lead to quantitative cap substitution. Indeed the ligand exchange occurs by simple incubation of the quantum rods in presence of an excess of the peptidic derivatives under basic conditions. The interaction between the semiconductor surface and the new coating molecule occurs through the three strongly interacting N-terminal cysteines and a very high packing density (≈0.6 nm^2/peptide) was obtained thanks to an alkyl chain inserted within the ligand structure in comparison to other

small 2014,
DOI: 10.1002/smll.201400300

NANO MICRO small

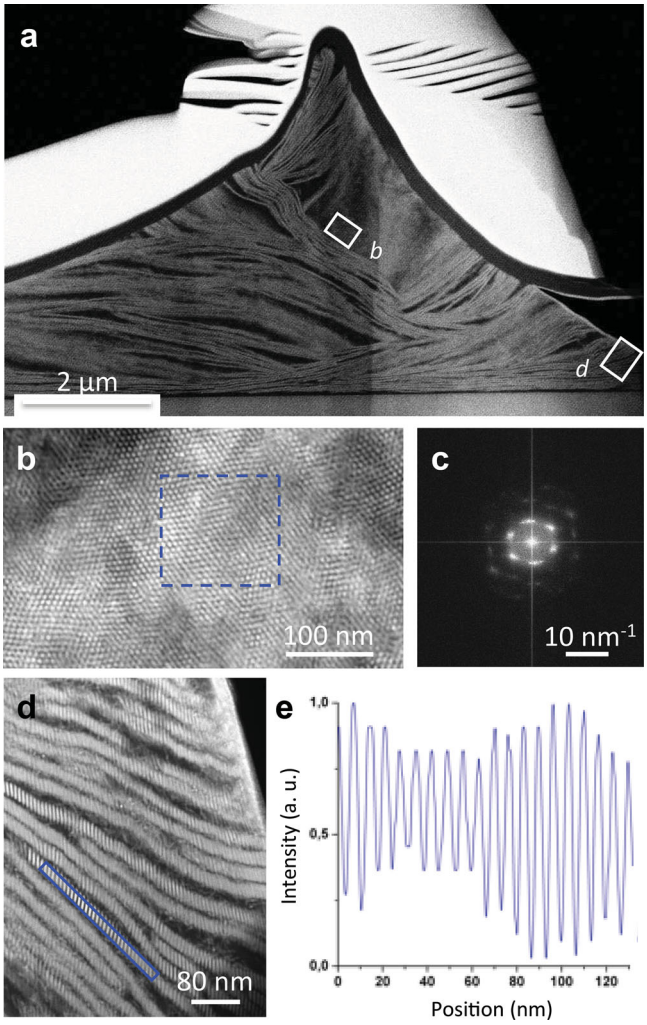

Figure 5. a) STEM-HAADF picture of a wall section cut by FIB normally to the ridge. b) Enlarged view evidencing some hexagonal packing parallel to the superstructure main axis. c) Fourier transform of the area contained in the blue dashed box. d) Zoom on a place where nanorods are organized in lamellae perpendicular to the wall. e) Intensity profile acquired along the blue continuous box.

kinds of ligands. In addition biomolecules can be covalently bound to the hydrophilic QR because of the presence of a carboxylic acid as terminal group in the ligand. Next, relying on fluorescence emission spectroscopy, electrophoresis, and DLS, we proved that the optical and colloidal properties of the CdSe/CdS nanorods dispersed in aqueous buffers are preserved for weeks until pH remains above 4 and ionic strength stays below or equal to 1 M. Such a result is due to both the PEG spacer and the carboxylic acid group present at the C-terminal peptide extremity. Finally, we evidenced the possibility to fabricate well-defined ordered superstructures from the obtained solution, just by allowing the water to evaporate. As an example, a regular network of micron size walls is produced over several millimeters squares when drying is performed between a flat substrate and a mold patterned with an array of pillars. EM images confirmed that particle organization yields a smectic B phase similar to the one identified by SAXS after bulk desiccation in a capillary tube. The correlation between the fluorescence properties of the QRs

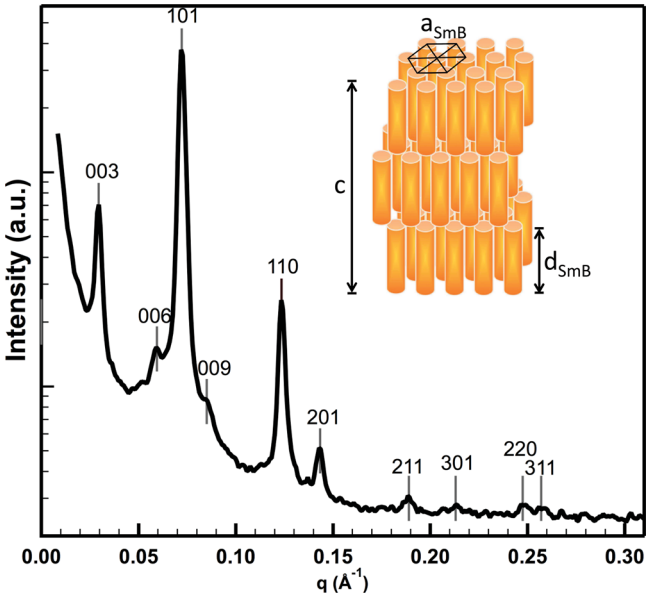

Figure 6. SAXS spectrum of an aqueous peptide-QR suspension dried in a capillary tube. The peak indexation corresponds to the smectic B organization represented in the upper right corner (see Table S1 for details).

and their organization within the supercrystals is currently under study and the results will be published elsewhere.

Our easy method for quantum rods capping and self-assembly thus leads to the formation of supracrystals densely packed, a result that appears to be a first step towards the elaboration of more sophisticated superstructures. Indeed, the use of PEGylated peptides offers the possibility to chemically adjust the interaction potential between the nano-objects, for instance by varying the charge density thanks to the introduction of appropriate functional groups. In a forthcoming paper, we will consequently present how to modulate QRs interdistance, alike what we have previously realized with gold nanorods.[6] Since this spacing parameter is of paramount importance to tune the final superstructure properties (e.g., the optical response under photo-irradiation), our studies will be relevant for integration in either photo-electrochemical[15c] or opto-electronical devices. Moreover, the ability to easily disperse in water and self-assemble nanorods provide a new issue for developing novel hybrid materials[31] and will allow us to combine semiconductor with metal particles inside dense and ordered features, in order to study phonon-plasmon coupling.[28] The high density of these materials can be exploited to modulate the performance of light harvesting devices for direct conversion of solar energy to produce fuel. For example the coupling with enzymes such as hydrogenase could serve to optimize the photo-electrocatalysis in fuel cells.[29]

4. Experimental Section

Chemicals: We purchased cadmium oxide (CdO, 99.998%), selenium (Se, 99.5%), and hexylphosphonic acid (HPA, 99%) from Alfa Aesar; sulfur (S, 99%) from Strem Chemical; trioctylphosphine

DOI: 10.1002/smll.201400300

oxide (TOPO, 99%), trioctylphosphine (TOP, 97%), octadecylphosphonic acid (ODPA, 97%), tetramethylammonium hydroxide (TMAOH, 25% w/w in methanol), and agarose (EEO 0.09–0.13) from Sigma-Aldrich. Peptides were synthetized and purified by HPLC (>90%) by Polypeptide (Strasbourg, France). The Britton and Robinson buffers with a constant ionic strength (20 mM) were prepared according to described protocols.[30]

CdSe/CdS Quantum Rods Synthesis: Following a procedure described by Carbone et al.,[21] CdSe seeds were obtained in a TOPO/TOP/ODPA mixture and CdSe/CdS core/shell nanorods were grown in a TOPO/TOP/ODPA/HPA mixture, both at 350 °C (see Supplementary Information for details). These as synthetized QRs were then washed by 3 centrifugation/redispersion cycles using a toluene/methanol (1/5) mixture and stored in a small amount of toluene until further use. In the following, the resulting purified particles are called "hydrophobic QRs".

Transmission Electron Microscopy: For morphological analysis a 1.5 µL droplet of diluted hydrophobic QR suspension, at ≈0.1 nM, was allowed to evaporate onto Formvar-carbon coated copper grids (Agar Scientific). Size histograms were then obtained from transmission electron microscopy images recorded on a JEOL 1400 operating at 120 kV. Conversely, for crystal structure determination the sample was prepared onto ≈50 nm thick silicon nitride membrane (DuraSiN) and Z-contrast images were acquired on an aberration-corrected JEOL 2200FS operating at 200 kV in scanning transmission electron microscopy (STEM) mode, using a high angle annular dark field (HAADF) detector. Images were then Fourier transformed relying on ImageJ.

Peptide Grafting: Just before functionalization the preceeding hydrophobic QRs were washed 3 more times in a similar way, in order to remove all ligands remaining in solution. The final redispersion was achieved in chloroform so as to obtain 30 µL aliquots at 10 mg/mL. The latter organic suspension was next mixed with 90 µL of 20 mM aqueous peptide solution, an addition followed by the one of 5 µL of TMAOH at 25% (w/w) in methanol. Transfer of the fluorescent particles from the organic phase to the aqueous one was then observed. After 15 min incubation, chloroform was subsequently allowed to evaporate at room temperature for 0.5 h. Ligands in excess were eventually removed by size exclusion chromatography using sephadex G-25 columns (NAP-5 or NAP-10 from GE Healthcare). In routine both column equilibration and elution were performed with ultra-pure water. However, for NMR experiments a borate buffer prepared in deutered water was used instead (1 M H_3BO_3, 1 M KCl, 1 M NaOH, uncorrected pH 9.0). In all cases it yielded an aqueous suspension of water-soluble nanorods, which is referred to as "peptide-QRs" in the rest of the article.

UV–Vis Absorption Spectroscopy: Measurements were achieved using a Cary 100 SCAN UV-Vis spectrometer (Varian) and 1 cm long quartz cuvettes. The concentration of QRs in the various suspensions was calculated as described in the literature, that is, relying on the absorbance at 350 nm as well as on the corresponding nanorod absorption coefficient $\varepsilon_{350} = 0.38 \times 10^{26}$ V mol^{-1}, where V is the particle volume in cm^3.[3c]

Fluorescence Spectroscopy: Emission spectra were recorded on a Fluorolog–3 fluorimeter (Horiba Jobin-Yvon). All samples were excited at their absorption maxima, which had previously been evaluated by UV-Vis spectrometry. In addition, to avoid self-absorption effects the optical density at the excitation wavelength was set between 0.01 and 0.1. The quantum yield of QRs, Φ_{QR}, was determined using the one of Rhodamine 6G dissolved in water as reference, $\Phi_{Rh} = 0.96$. More precisely, we relied on $\Phi_{QR} = \Phi_{Rh} (I_{QR}\ OD_{Rh}\ n_{QR}^2)/(I_{Rh}\ OD_{QR}\ n_{Rh}^2)$ where n is the solution refractive index, I is the integrated fluorescence intensity, and OD the optical density; the "QR" and "Rh" subscripts refer to the measurements on QRs and Rhodamine 6G, respectively.[33]

Gel Electrophoresis: Charge variations resulting from the functionalization of QRs with peptides, as well as possible aggregation phenomena, were monitored by electrophoresis in a 0.5% agarose gel prepared in 0.02 M KCl, 0.02 M H_3BO_3, 0.02 M NaOH, 0.015 M NaCl buffer, pH 8.2. Loading was performed in 3% w/v glycerol, a 50 V cm^{-1} electric field was applied for 45 min, and visualization was achieved on a 350 nm transilluminator.

Dynamic Light Scattering (DLS): QR colloidal stability was accessed from measurements performed at an angle of 173° on a Zetasizer Nano ZS (Malvern Instruments). All solutions were filtered through 0.2 µm Millipore filters (Millex HV) and samples were kept sealed all along time series. Data were collected at 25 °C. Only an analysis for spherical nanoparticles can be implemented on this apparatus; therefore, the extracted hydrodynamical diameter is just a rough estimate giving information on colloidal stability but not providing fine details on object shape.

Fourier Transformed Infrared (FTIR) Spectroscopy: Characterizations were carried out on a 640-IR apparatus (Varian) using the attenuated total reflectance (ATR) mode. Samples were prepared as a powder by either evaporation of the solvent for hydrophobic QRs dissolved in chloroform or by lyophilization for peptide-QRs in solution in ultra pure water.

Nuclear Magnetic Resonance (NMR) Spectroscopy: ^{31}P NMR spectra were recorded at 298 K on a Bruker Avance 500 MHz spectrometer equipped with a 5 mm HR-MAS triple-resonance probe head (PRISM platform, Rennes 1 University, France). The spectral width was 100 kHz, centered at –15.6 ppm. A 1D sequence with power-gated decoupling using a 30 degrees flip angle was applied. The acquisition parameters were the following: 32 k points time domain, 2 s relaxation delay, 2 dummy scans, 240 to 5 k scans. Spectra were then transformed with 16 k points. Proton NMR was achieved at 278 K on an ultrashield Bruker Avance spectrometer operating at 500 MHz and equipped with a 5 mm TXI inverse triple-resonance cryoprobe head (PRISM platform, Rennes 1 University, France). A spectral width of 12 ppm centered on water resonance was used. Water suppression was realized either by water-presaturation or gradient-based sequences.[34] The 2D spectra were recorded by using standard Bruker sequences. Acquisitions were performed in echo-anti-echo mode with Z-gradients selection. Mixing times of 100 ms for TOCSY and 250 ms for NOESY were used. Diffusion coefficients were determined relying on the Stejskal–Tanner PFG-SE sequence.[35] Sixteen acquisitions were recorded by increasing the strength of the gradient field applied along the tube main axis, while all the other parameters were kept constant (3 s relaxation delay, 8 scans, 16 k time domain). Gradient pulses were 5 ms long, with a 150 ms delay between them. After Fourier Transform, integration of resonance peaks was used for diffusion coefficient determination.

X-Ray Scattering: Peptide-QRs in suspension at 1 µM in ultrapure water were loaded in 1.3–1.6 mm round glass capillaries (Glas Technik & Konstruktion Müller & Müller OHG) and samples were allowed to dry under vacuum at 150 mBar during one week in the presence of P_2O_5. Experiments on hydrophobic QRs were

small 2014,
DOI: 10.1002/smll.201400300

achieved in a similar way: hydrophobic QRs from the same synthesis batch were dissolved in either chloroform or toluene at 1 μM, injected in the capillary, and dried under vacuum. Small angle X-ray scattering (SAXS) measurements were performed on the high brilliance SWING beam line at the Soleil synchrotron facility, with monochromators set at 12 KeV.[32,36] Using a CCD detector at 1.2 m from the capillary, diffraction patterns were recorded for reciprocal spacing $q = 4\pi \sin(\theta)/\lambda$ varying between 0.01 and 0.8 $Å^{-1}$, that is, repetitive distances $d = 2\pi/q$ ranging from 628 to 78 Å. All samples exhibited powder diffraction patterns that could be submitted to circular integration to yield scattered intensity plots.

Nanorod Walls Self-Assembly: A PDMS stamp (Sylgard 184, Dow Corning) was first cast on a master mold that had been photolithographed in SU8–2025 (Microchem). The elastomer surface displayed 35 μm high and 100 μm large pillars, arranged on a square lattice of parameter 175 μm. A droplet of peptide-QR suspension, at 2.5 μM in ultra pure water and supplemented with Tween 20 at 96.4 μM, was then sandwiched in between a flat silicon wafer and the micropatterned template. After drying for 12 h at room temperature, the PDMS lid was removed in order to proceed to observations.

Electron Microscopy of Superstructures: The 3D organization of the colloidal assemblies was first observed by scanning electron microscopy (SEM) using a Magellan 400 L (FEI) equipped with a field emission gun and running at the voltage acceleration of 15 kV with a 0.2 nA probe current. Settings and procedures were similar to the ones used for your previous work on gold nanorods,[6] except that no micromanipulator was necessary to break open the structures and that the higher acceleration voltage enabled us to obtain good views although some organic film was initially present at the feature surface. Alternatively, to gain insight on wall interior we relied on STEM-HAADF investigations performed on the JEOL 2200FS once again operating at 200 kV. The key point was here to achieve a successful preparation of thin sections of QR supracrystal: the dried structures were first protected with ≈500 nm of carbon by rod evaporation in a Q150T ES coating system (Quorum Technologies) and ≈1–2 μm of platinum by $C_9H_{16}Pt$ cracking in a STRATA DB 235 focus ion beam (FIB) machine (FEI). Then, a slice of superstructure was cut out perpendicular to the ridge using the gallium FIB (see Figure S8, Supporting Information), extracted with the micromanipulator, thinned up to electron transparency at low intensity, and cleaned at low voltage.

Supporting Information

Supporting Information is available from the Wiley Online Library or from the authors. Detailed protocols are given for the synthesis of the CdSe/CdS nanorods and for the NMR experiments. Figure S1: TEM, STEM-HAADF and spectroscopic characterization of the hydrophobic QRs. Figure S2: Chemical structure of TCCPAC (numbered protons) and its assigned 1H NMR proton spectrum in water at pH 7.0. Figure S3: Overlay of 2D1H NMR spectra of TCCPAC in 10% D2O, pH 7.0. Figure S4: 1H NMR proton spectra of TCCPAC-QRs during the purification step in deuterated borate buffer, pH 9.0. Figure S5: Overlay of 1H DOSY spectra of TCCPAC-QRs and free TCCPAC. Figure S6: Chemical structure of TCCPAM and agarose gel electrophoresis of QRs capped with different TCCPAC/TCCPAM ratios. Figure S7: Chemical structure of TCPAC and evolution in time of the TCCPAC-QRs fluorescence and hydrodynamical diameter. Figure S8: SEM pictures showing where the wall was cut by FIB technique. Figure S9: SAXS spectrum of hydrophobic QRs dried in a capillary from a suspension in toluene. Table S1: STEM-HAADF image analysis confirming the crystal composition of the CdS shell and CdSe core. Table S2: Indexation of the Smectic B crystal obtained from a dried suspension of TCCPAC-QRs.

Acknowledgements

V.M. and F.A. thank the Région Bretagne and the Direction Générale de l'Armement for the PhD fellowships of T.B., M.P., and C.H. V.M. and C.G. acknowledge the Agence Nationale de la Recherche for financial support through the "Biomodulator" grant obtained in 2008 on the PNANO program. C.G. also benefited from a financial support from the Cnano IdF, in the context of the DyPMOA project. The authors are indebted to A. Burel for her technical support during observations on the TEM platform Mric-UMS 3480-biosit-Université de Rennes 1 and to X. Zhao for assistance with sample preparation prior to FIB processing.

[1] a) J. Hu, L.-s. Li, W. Yang, L. Manna, L.-W. Wang, A. P. Alivisatos, *Science* **2001**, *292*, 2060; b) D. V. Talapin, E. V. Shevchenko, C. B. Murray, A. Kornowski, S. Förster, H. Weller, *J. Am. Chem. Soc.* **2004**, *126*, 12984; c) A. Rizzo, C. Nobile, M. Mazzeo, M. D. Giorgi, A. Fiore, L. Carbone, R. Cingolani, L. Manna, G. Gigli, *ACS Nano* **2009**, *3*, 1506; d) Y. Luo, L.-W. Wang, *ACS Nano* **2009**, *4*, 91; e) M. Zanella, R. Gomes, M. Povia, C. Giannini, Y. Zhang, A. Riskin, M. Van Bael, Z. Hens, L. Manna, *Adv. Mater.* **2011**, *23*, 2205.

[2] C. Hamon, A. Ciaccafava, P. Infossi, P. Even-Hernandez, E. Lojou, V. Marchi, *Chem. Comm.* **2014**, *50*, 4989.

[3] a) D. V. Talapin, R. Koeppe, S. Götzinger, A. Kornowski, J. M. Lupton, A. L. Rogach, O. Benson, J. Feldmann, H. Weller, *Nano Lett.* **2003**, *3*, 1677; b) L. Amirav, A. P. Alisivatos, *J. Phys. Chem. Lett.* **2010**, *1*, 1051; c) R. Alam, D. M. Fontaine, B. R. Branchini, M. M. Maye, *Nano Lett.* **2012**, *12*, 3251.

[4] R.-Q. Song, H. Cölfen, *Adv. Mater.* **2010**, *22*, 1301.

[5] R. Tang, H. Lee, S. Achilefu, *J. Am. Chem. Soc.* **2012**, *134*, 4545.

[6] C. Hamon, M. Postic, E. Mazari, T. Bizien, C. Dupuis, P. Even-Hernandez, A. Jimenez, L. Courbin, C. Gosse, F. Artzner, V. Marchi-Artzner, *ACS Nano* **2012**, *6*, 4137.

[7] a) K. T. Yong, J. Qian, I. Roy, H. H. Lee, E. J. Bergey, K. M. Tramposch, S. He, M. T. Swihart, A. Maitra, P. N. Prasad, *Nano Lett.* **2007**, *7*, 761; b) K. T. Yong, R. Hu, I. Roy, H. Ding, L. A. Vathy, E. J. Bergey, M. Mizuma, A. Maitra, P. N. Prasad, *ACS Appl. Mater.and Interfaces* **2009**, *1*, 710; c) D. Sun, O. Gang, *Langmuir* **2013**, *29*, 7038–7046.

[8] S. Deka, A. Quarta, M. G. Lupo, A. Falqui, S. Boninelli, C. Giannini, G. Morello, M. De Giorgi, G. Lanzani, C. Spinella, R. Cingolani, T. Pellegrino, L. Manna, *J. Am. Chem. Soc.* **2009**, *131*, 2948.

[9] R. Kumar, H. Ding, K.-T. Yong, I. Roy, E. J. Bergey, P. N. Prasad, *Chem. Mater.* **2010**, *22*, 2261.

[10] K. A. Brown, M. B. Wilker, M. Boehm, G. Dukovic, P. W. King, *J. Am. Chem. Soc.* **2012**, *134*, 5627.

DOI: 10.1002/smll.201400300

[11] A. Dif, F. Boulmedais, M. Pinot, V. Roullier, M. Baudy-Floc'h, F. M. Coquelle, S. Clarke, P. Neveu, F. Vignaux, R. L. Borgne, M. Dahan, Z. Gueroui, V. Marchi-Artzner, *J. Am. Chem. Soc.* **2009**, *131*, 14738.
[12] J. M. Tsay, S. Doose, F. Pinaud, S. Weiss, *J. Phys. Chem. B* **2005**, *109*, 1669.
[13] A. Dif, E. Henry, F. Artzner, M. Baudy-Floc'h, M. Schmutz, M. Dahan, V. Marchi-Artzner, *J. Am. Chem. Soc.* **2008**, *130*, 8289.
[14] B. C. Mei, K. Susumu, I. L. Medintz, H. Mattoussi, *Nat. Protoc.* **2009**, *4*, 412.
[15] a) J. B. Delehanty, C. E. Bradburne, K. Susumu, K. Boeneman, B. C. Mei, D. Farrell, J. B. Blanco-Canosa, P. E. Dawson, H. Mattoussi, I. L. Medintz, *J. Am. Chem. Soc.* **2011**, *133*, 10482; b) G. Rainö, T. Stoferle, I. Moreels, R. Gomes, Z. Hens, R. F. Mahrt, *ACS Nano* **2012**, *6*, 1979; c) Z. Han, F. Qiu, R. Eisenberg, P. L. Holland, T. D. Krauss, *Science* **2012**, *338*, 1321.
[16] C. Burda, X. Chen, R. Narayanan, M. A. El-Sayed, *Chem. Rev.* **2005**, *105*.
[17] J. M. Tsay, S. R. Doose, S. J. Weiss, *J. Am. Chem. Soc.* **2006**, *128*.
[18] T. Bala, A. Sanyal, A. Singh, D. Kelly, C. O'Sullivan, F. Laffir, K. M. Ryan, *J. Mater. Chem.* **2011**, *21*, 6815.
[19] R. Gomes, A. Hassinen, A. Szczygiel, Q. Zhao, A. Vantomme, J. C. Martins, Z. Hens, *J. Phys. Chem. Lett.* **2011**, *2*, 145.
[20] B. Valeur, *Molecular Fluorescence: Principles and Applications*, Wiley-VCH, Weinheim **2001**.
[21] L. Carbone, C. Nobile, M. De Giorgi, F. D. Sala, G. Morello, P. Pompa, M. Hytch, E. Snoeck, A. Fiore, I. R. Franchini, M. Nadasan, A. F. Silvestre, L. Chiodo, S. Kudera, R. Cingolani, R. Krahne, L. Manna, *Nano Lett.* **2007**, *7*, 2942.
[22] J. Israelachvili, *Intermolecular and Surface Forces*, Academic Press, New York **1992**.
[23] a) Z. Hens, J. C. Martins, *Chem. Mater.* **2013**, *25*, 1211; b) H. Virieux, M. Le Troedec, A. Cros-Gagneux, W.-S. Ojo, F. Delpech, C. Nayral, H. Martinez, B. Chaudret, *J. Am. Chem. Soc.* **2012**, *134*, 19701.
[24] B. Fritzinger, R. K. Capek, K. Lambert, J. C. Martins, Z. Hens, *J. Am. Chem. Soc.* **2010**, *132*, 10195.
[25] J. S. Owen, J. Park, P.-E. Trudeau, A. P. Alisivatos, *J. Am. Chem. Soc.* **2008**, *130*, 12279.
[26] I. Moreels, B. Fritzinger, J. C. Martins, Z. Hens, *J. Am. Chem. Soc.* **2008**, *130*, 15081.
[27] E. Henry, A. Dif, M. Schmutz, L. Legoff, F. Amblard, V. Marchi-Artzner, F. Artzner, *Nano Lett.* **2011**, *11*, 5443.
[28] D. Sun, O. Gang, *J. Am. Chem. Soc.* **2011**, *133*, 5252.
[29] C. Hamon, A. Ciaccafava, P. Infossi, P. Even-Hernandez, E. Lojou, V. Marchi, *Chem. Comm.* **2014**.
[30] J. A. C. Frugoni, *Gazz. Chim. Ital.* **1957**, *87*, 403.
[31] M. Artemyev, B. Müller, U. Woggon, *Nano Lett.* **2003**, *3*, 509.
[32] W. van Grondelle, C. López Iglesias, E. Coll, F. Artzner, M. Paternostre, F. Lacombe, M. Cardus, G. Martinez, M. Montes, R. Cherif-Cheikh, C. Valéry, *J. Struct. Biol.* **2007**, *160*, 211.
[33] J. R. Lakowicz, *Principles of Fluorescence Spectroscopy*, Springer, New York **2009**.
[34] a) T. L. Hwang, A. J. Shaka, *J. Magn. Reson., Ser. A* **1995**, *112*, 275; b) V. Sklená , M. Piotto, R. Leppik, V. Saudek, *J. Magn. Reson., Ser. A* **1993**, *102*.
[35] E. O. Stejskal, J. E. Tanner, *J. Chem. Phys.* **1965**, *42*, 288.
[36] G. David, J. Perez, *J. Appl. Crystallogr.* **2009**, *42*, 892.

Received: February 4, 2014
Revised: April 28, 2014
Published online:

DOI: 10.1002/smll.201400300